Journal of Applied Geophysics 159 (2018) 16–22

Contents lists available at ScienceDirect

Journal of Applied Geophysics

journal homepage: www.elsevier.com/locate/jappgeo

Q-estimation using seismic interferometry from vertical well data

Feng Cheng [a], Deyan Draganov [b,*], Jianghai Xia [c], Yue Hu [a], Jianhuan Liu [b]

[a] Subsurface Imaging and Sensing Laboratory, Institute of Geophysics and Geomatics, China University of Geosciences in Wuhan, 388 Lumo Rd., Wuhan, Hubei 430074, China
[b] Department of Geoscience and Engineering, Delft University of Technology, Stevinweg 1, 2628, CN, Delft, The Netherlands
[c] School of Earth Sciences, Zhejiang University, 38 Zheda Road, Hangzhou, Zhejiang 310027, China

ARTICLE INFO

Article history:
Received 7 July 2017
Received in revised form 2 May 2018
Accepted 31 July 2018
Available online 08 August 2018

Keywords:
Seismic interferometry
Intrinsic losses
Quality factor
Ghost reflection
Vertical well
Horizontal well
Numerical modelling

ABSTRACT

The Green's function between two receivers can be retrieved using seismic interferometry (SI) by cross-correlation, as if one of the receivers were a virtual seismic source. When the wavefields experience intrinsic losses during propagation, non-physical arrivals (ghosts) would appear in the retrieved result. These ghosts are a result of internal reflections inside the different layers lying between the subsurface sources and the receivers. Recent studies have introduced a stable method to monitor the layer-specific changes in quality factor (Q) using the ghosts retrieved by SI applied to a horizontal-well data. However, drilling a horizontal well is much more complicated and expensive than drilling a conventional vertical well. Because of this, we show here how the Q-estimation method introduced for the horizontal well can be adapted to monitor layer-specific changes of Q using a vertical well. In order to improve the accuracy of the Q-estimation, we propose a grid-searching method to detect the optimal effective Q. We illustrate our method using numerically modelling data from a horizontal and a vertical well.

1. Introduction

Estimation of the quality factor (Q) has a great potential to enhance our knowledge of rock properties. Furthermore, reliable Q-estimation is a prerequisite for standardized inverse Q-filters used to compensate for the anelastic attenuation of the seismic waves. In spite of the broad variety of available methods for Q-computation, only a few techniques, such as the spectral-ratio method and the central-frequency-shift method, are widely accepted. Still, even these two methods suffer from the problem of instability.

For example, the spectral-ratio (SR) method directly compares frequency spectra of two waveforms (McDonal et al., 1958; Hauge, 1981; Stainsby and Worthington, 1985; Tonn, 1991). However, it often appears unstable in practice because of fluctuations inherent in the frequency spectrum of any individual waveform (White, 1992; Parolai, 2014). The central-frequency-shift method estimates the shifting quantity of the central or peak frequency from a reference signal to analysis the change of the Q-values (Quan and Harris, 1997; Liu et al., 1998; Zhang and Ulrych, 2002; Matsushima et al., 2016). This method, which also depends on individual waveforms, is not stable either as it is strongly depends on the variation of the signal-to-noise ratio in the spectra. Wang (2014) improved the stability by conducting Q-analysis on an integrated observation. As follows from the above, development of a robust method for Q-estimation is important.

Recently, Draganov et al. (2010) proposed an alternative method for estimating effective Q-values. They showed how the layer-specific changes in velocity and Q can be estimated and monitored using non-physical arrivals (ghosts) in the results retrieved from seismic interferometry (SI). It has been shown that the Green's function between two receivers can be retrieved using seismic interferometry by cross-correlation, as if one of the receivers were a virtual seismic source (e.g., Campillo and Paul, 2003; Schuster et al., 2004; Snieder, 2004; Wapenaar and Fokkema, 2006). For the correct retrieval of the Green's function, it is assumed that the two receivers are illuminated homogeneously by sources along a boundary enclosing the receivers. The utilization of cross-correlation also assumes that the propagating waves are not subjected to intrinsic losses. This is hardly the case for measurements in the field. Still, SI by cross-correlation can be applied even in medium with intrinsic losses and still retrieve the correct Green's function if the source distribution in the medium is not only along a surface, but inside the complete volume surrounding the receivers (Snieder, 2007). The later is also not achievable in field measurements for exploration and production. Several studies have shown the effects of the intrinsic losses on the results retrieved from SI by cross-correlation (e.g., Draganov et al., 2010, 2013). When multiple scattering occurs in the lossy medium inside layers, the cross-correlation gives rise to ghosts in the retrieved response. To use the retrieved ghosts to estimate the layer-specific velocity and Q, as proposed by

* Corresponding author at: Department of Geoscience & Engineering, Delft University of Technology, Stevinweg 1, 2628, CN, Delft, The Netherlands.
E-mail addresses: marscfeng@cug.edu.cn (F. Cheng), d.s.draganov@tudelft.nl (D. Draganov), jhxia@zju.edu.cn (J. Xia), huyue0716@foxmail.com (Y. Hu), j.liu-4@tudelft.nl (J. Liu).

https://doi.org/10.1016/j.jappgeo.2018.07.019
0926-9851/

Draganov et al. (2010), sufficiently long recordings are needed to capture enough multiple scattering from inside the layers. When the recordings are insufficiently long, Ruigrok (2012) proposed as a remedy to utilize only the earliest such arrivals to estimate the Q above and the reflection coefficient at the top of the specific ghost-producing layer. Draganov et al. (2015) showed how the SI method of Ruigrok (2012) can be adapted to surface waves reflected from subvertical interfaces to estimate the quality factor of the medium and the reflection coefficient at the subvertical interface. The authors showed that recordings from two transient sources on both sides of the two receivers are required.

According to Draganov et al. (2010), the SI method could act as an alternative and stable method for Q-estimation. However, for that are required sources in the subsurface that illuminate the receivers with a comparable energy. Draganov et al. (2013) proposed in practice to use recordings from a horizontal well. The authors showed that to utilize effectively the ghosts, they should be identified and further connected to the specific subsurface layers that cause them to arise. The identification and connection was achieved using data from a vertical well.

It is well known that drilling a horizontal well is a more complicated process than drilling a conventional vertical well. Compared to a vertical well, the horizontal well costs much higher. Using the current technology, a new horizontal well in the USA drilled from the surface costs 1.5 to 2.5 times more than a vertical well. A re-entry horizontal well costs about 0.4 to 1.3 times a vertical-well cost (Joshi, 2003). That is why, it is desirable to obtain the same or similar results in Q-estimation with ghost arrivals from vertical-well data, rather than from horizontal-well data.

In the following, we show how the method from Draganov et al. (2013) can be adapted and applied to estimate the layer-specific Q-values in the subsurface from vertical-well data. First, we apply the SI method to synthetic seismic data from a horizontal-well geometry to review how to ghost arrivals are used for Q-estimate of specific layers. In order to improve the accuracy of the Q-estimation, we propose a quantitative method – 1-D grid searching – for the Q-compensation procedure. Next, we present how to use polarity change of the retrieved ghost events to estimate Q-values in a vertical-well geometry. Finally, we conduct a comparison to summarize the advantages of the improved SI method using the vertical-well data. In fact, this work can be seen as a continuation of to the SI method for Q-estimation described in Draganov et al. (2013), and we refer the reader to the specific literature for more details.

2. Finite-difference modelling for seismic interferometry

We closely follow Draganov et al. (2013) to simulate a transmission experiment using a 2-D acoustic finite-difference modelling scheme (Thorbecke and Draganov, 2011). The first derivative of a Gaussian wavelet with a centre frequency of 40 Hz is used as a source signature. In the finite-difference modelling, we select a free surface for the top boundary and perfectly matched layer absorbing-boundary conditions are selected for the other three boundaries to avoid edge reflection (Chew and Liu, 1996; Drossaert and Giannopoulos, 2007).

Fig. 1 shows the model we used to simulate seismic recordings from an impulsive source at the surface to receivers along a vertical well. For a base survey, the model is given with a velocity of $Q_p^3 = 1800m/s$, and a quality factor $Q_p^3 = 80$ in the third (reservoir) layer. Note, that using only one surface source aims to reflect the fact that in practice the surface-source aperture might be very limited. A dipole source at the surface is located at 4000 m horizontal distance. The horizontal well is instrumented between 3000 m and 5000 m, with receivers placed every 20 m. The receivers in the vertical well are deployed between depth levels of 100 mm and 1090 m at a 15-m interval. The vertical component of the particle velocity is recorded for the receivers in both the horizontal well and the vertical well.

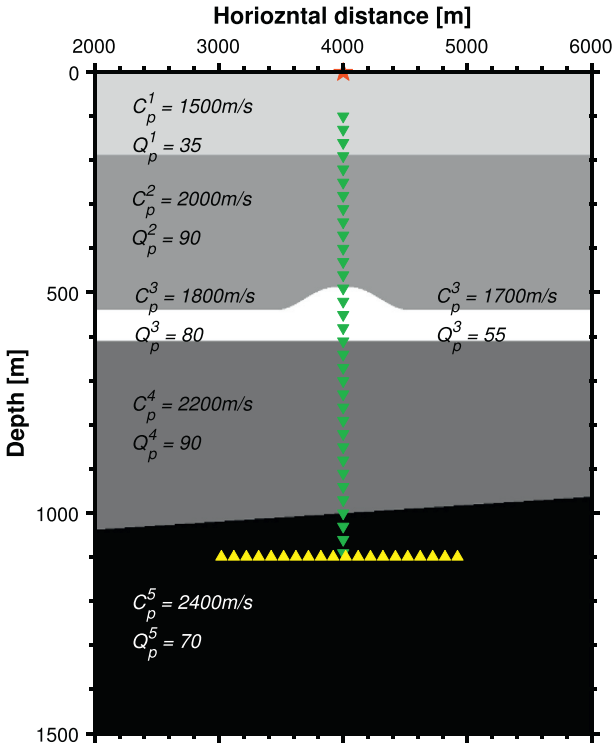

Fig. 1. Subsurface model with receivers installed along a vertical (green triangles) and a horizontal (yellow triangles) well. The vertical well is instrumented between depths of 100 m and 1090 m every 15 m, the horizontal well is instrumented between 3000 m and 5000 m horizontal distance every 20 m. The propagation velocity in the layers is denoted by C_p, while Q stands for quality factor. (For interpretation of the references to colour in this figure legend, the reader is referred to the web version of this article.)

Responses with a length of 4 s are recorded along the two wells from the same source located at the surface. The time sampling is 2 ms. The modelled recordings are shown in Fig. 2:a-b. In them, we can see the reflections from the horizontal and inclined layer boundaries and their multiples, e.g., the linear inclined events in Fig. 2:b, but also the effects of the anticline, e.g., the hyperbolic-like events in Fig. 2:b. We perform SI by taking the autocorrelation of each trace in the horizontal well Fig. 2:c and the vertical well Fig. 2:d. Using the horizontal well alone, it is ambiguous to identify the retrieved ghosts due to the intrinsic losses and connect them to the specific layers that cause them to appear. Therefore, Draganov et al. (2013) proposed to make use of a vertical-well geometry to achieve the identification, and then to proceed with the Q-estimation using the horizontal well. We can easily distinguish the retrieved ghosts from the retrieved physical events by the changing polarity of the ghost events along the receivers in the vertical well. For example, the four horizontal events retrieved at 0.13 s, 0.30 s, 0.35 s, and 0.43 s are ghosts. More details about how to identify the ghosts will be illustrated in the following sections.

3. Grid searching for Q-estimation

We apply SI by autocorrelating all traces in the transmission panel of the horizontal well (Fig. 2:a) and then summing the autocorrelation results (Fig. 3:a) together to obtain a zero-offset reflection trace for a source and receiver at the surface (Fig. 3:b). The SI theory requires summation (integration) over a closed boundary. As we do not have a closed subsurface-receiver boundary, we taper the autocorrelations gradually to zero for receivers at both ends (Draganov et al., 2013).

Using the results of applying SI to the data from the vertical well, which will be demonstrated later, we can unambiguously interpret the ghosts and thickness of the second (0.3 s, 300 m), third (0.13 s, 120 m) and fourth (0.35 s, 390 m) layers. Based on this information,

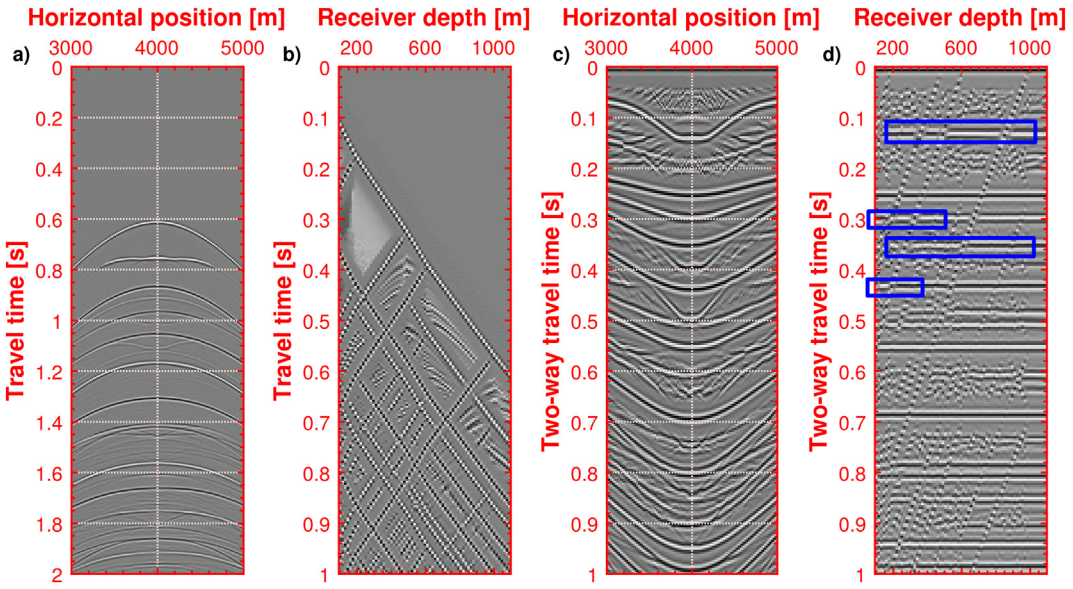

Fig. 2. Synthetic records of the base survey before and after seismic interferometry. Synthetic transmission wavefield from a source at the surface recorded by receivers in (a) the horizontal well and (b) the vertical well. (c) and (d) present the corresponding result of applying seismic interferometry by autocorrelation to each trace in (a) and (b), respectively. The blue boxes show the ghost arrivals with polarity reversal. (For interpretation of the references to colour in this figure legend, the reader is referred to the web version of this article.)

we are be able to estimate the layer-specific Q-values and/or velocities.

We apply a gain of $e^{\frac{\pi f_0}{Q_{trial}}}$ (Aki and Richards, 2002) (where f_0 is the centre frequency of the source wavelet) to the transmission panel (Fig. 2:a) to proceed with the Q-compensation procedure of Draganov et al. (2010) to estimate the effective Q-value of the overburden above a ghost-producing layer. For a Q_{trial} equal to the effective Q-value of the overburden above a specific ghost-producing layer, the ghost arrival should disappear in the retrieved zero-offset reflection trace (Fig. 3:b).

The Q-estimation procedure in Draganov et al. (2010, 2013) is, strictly speaking, a qualitative method. The authors introduced the Q-estimation method on synthetic data and demonstrated that the method works by testing it for a few Q_{trial} values some of which were chosen to be away from the true values and some to be the true values. In this work, we present a quantitative method for the Q-compensation procedure – we use 1-D grid searching. First, we apply a series of scanning Q^i_{trial}, $i = 1...M$ ($M = trial\ \ number$) to compensate each trace in the transmission panel before application of SI. Next, we compute the maximum absolute amplitude inside a time window around the ghost arrivals for each retrieved response:

$$\alpha^i_j = max\left\{|A^i_j(t)|\right\}, \tag{1}$$

where, $A^i_j(t)$ denotes the amplitude compensated with Q^i_{trial} for the retrieved response at the j^{th} trace, $j = 1...N$ ($N = trace\ number$); t denotes the time window between with the ghost arrivals. Finally, we compute the mean of all the maximum absolute amplitudes:

$$\varepsilon^i = \sum_{j=1}^{N} \alpha^j / N. \tag{2}$$

When the scanning Q^i_{trial} increases and becomes close to the correct Q-value, the ghost should disappear and ε^i decreases, while when Q^i_{trial} passes the correct Q-value and increases further, the ghost should

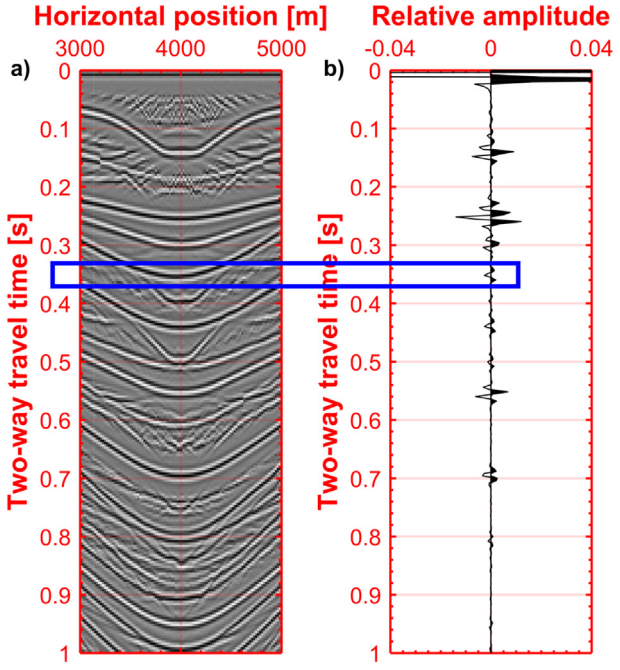

Fig. 3. (a) The autocorrelated traces from the horizontal well of the base survey (repeated from Fig. 2:a). (b) The retrieved zero-offset reflection trace by summing the autocorrelations in (a) together.

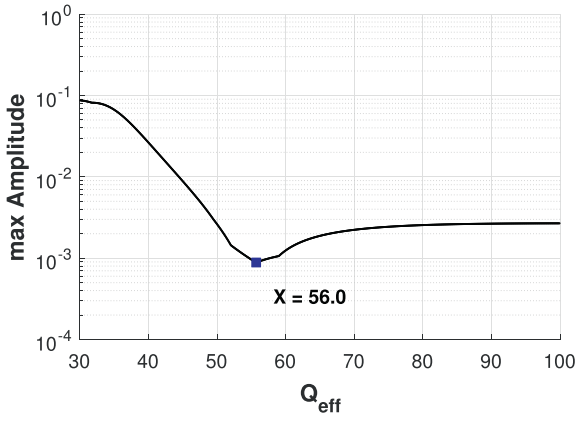

Fig. 4. The obtained relationship between the scanning Q_{trial} and the maximum amplitude ε for the retrieved ghost at 0.35 s using the data from the horizontal well.

reappear and ε^i increases again (Draganov et al., 2013). Therefore, we pick the optimal Q_{trial} at the lowest point in the $Q_{trial} - \varepsilon$ diagram as the effective Q of the overburden above a specific ghost-producing layer. Fig. 4 shows the relationship between the scanning Q_{trial} and the maximum absolute amplitude ε for the ghost at 0.35 s; the graph also indicates the chosen effective $Q_{eff}^{trial} = 56.0$ of the overburden down to the fourth layer, which is very close to the theoretically calculated value $Q_{eff} = 56.3$. For a Q_{trial} equal to the effective Q of the overburden above the fourth layer, the ghost arrival at 0.35 s in Fig. 5 disappears, while the amplitude of the physical events improves, as the yellow box in Fig. 5 highlights. The identified ghost arrival at 0.13 s has also been mostly attenuated, which means the effective Q-value above the third layer is close to the value for the effective Q above the fourth layer. Note that we take the physical event around 0.25 s (blue box in Fig. 5) as reference to normalize Fig. 5:a and Fig. 5:b (as well as the following Fig. 7), in order to compare the change in the amplitudes before and after the Q-compensation.

We suppose that the proposed grid-searching method for the Q-compensation is valid, and possess the ability to be adapted for complex real-world applications. For example, we simply compute the mean of the maximum absolute amplitude as a scanning parameter ε in this work, but we could also compute the standard deviation of the maximum amplitude instead, in which case the relationship between Q_{trial} and ε would be different.

4. Q-estimation using a vertical well

Fig. 6:a shows the retrieved responses from the base-survey data of the vertical well (zoomed Fig. 2:d). According to Draganov et al. (2013), we could easily identify the horizontal ghost arrivals as such because they display polarity reversal at the top of the ghost-producing layer, as the red circles in Fig. 6:a indicate. With these polarity-reversal points, we could determine the position of the layer interfaces or the thickness of each layer, and the velocity of each layer with a quasi-1-D assumption of the medium. Therefore, we are able to describe the kinematic representation for the identified non-physical events (Fig. 6:a) as if they were recorded with coinciding source and receiver at the position of the top of the ghost-producing layer. On the other hand, we can also see the inclined non-physical arrivals which are retrieved from the correlation of arrivals coming to the receivers from opposite directions. Based on the information obtained from the horizontal ghosts, we could also describe the kinematic representations for the inclined non-physical arrivals (Fig. 6:b) as if they were recorded with coinciding source and receiver at the position of the receiver inside the well.

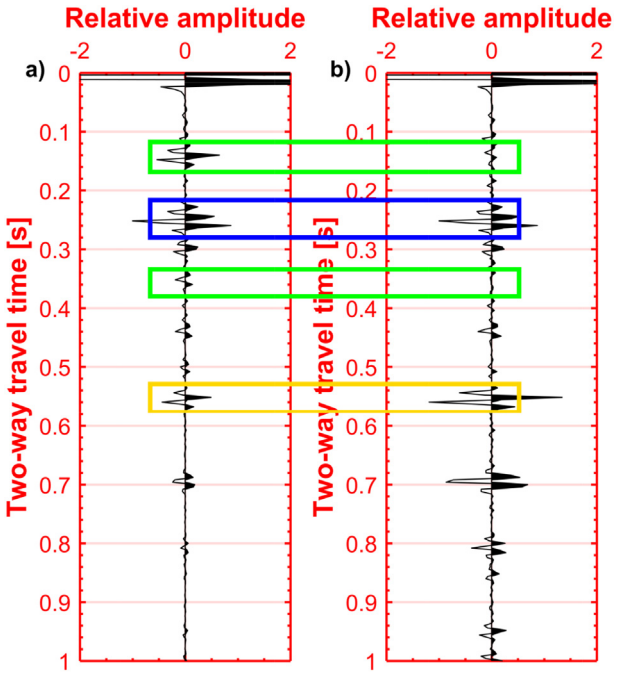

Fig. 5. The retrieved zero-offset reflection trace (a) before and (b) after Q-compensation with the detected $Q_{trial} = 56.0$ from Fig. 4.

To develop a method for Q-estimation using the identified horizontal ghosts in a vertical well, we adapt the Q-compensation procedure of Draganov et al. (2010). Instead of compensating all traces as we did above for the horizontal well, we divide the transmission panel into two parts: a part containing the autocorrelations above a specific ghost-producing layer (the magenta box in Fig. 6:a) called UP part, and a part containing several trace from inside the ghost-producing layer from receivers close to the upper interface of the ghost-producing layer (white box in Fig. 6:a) called DOWN part. As described above, the polarity-reversal point arises at the upper interface of the ghost-producing layer. Therefore, the retrieved responses of the UP part are characterized by polarity opposite to that of the DOWN part. If we sum the mean values of the retrieved responses after application of Q-compensation to both parts (in the magenta box and the white box), the ghost event should be eliminated. This happens because these two mean terms after compensation would possess the same amplitude but opposite polarity due to the intrinsic losses inside the ghost window. To calculate the mean term of the DOWN part, in this work we choose five traces. If this is allowed by the specific geometry of a field data, this is a preferred way of calculation as it would decrease the dependence on the signal-to-noise ratio of individual traces. Theoretically, even just a single trace in the DOWN part could be used, for example when the geophones in the well sample the layer coarsely close to the upper interface of the ghost-producing layer. The risk in such cases, though, is that due to low signal-to-noise ratio an erroneous Q might be estimated. This problem might be avoided if a decision is taken to monitor changes only at specific layers, for example a reservoir and the overburden close above it. This would allow for denser sensor deployment and still keeping the costs low. An even better solution would be to instrument the vertical well with a distributed acoustic sensing (optical fiber). We think that the method we introduced here will be especially helpful for data from such systems. The variability of the polarity of the horizontal ghost inside the UP part will influence the Q-estimation as well. The variability is due to interference with other retrieved events. To counter such variability, we choose an UP part a bit longer than the DOWN part t to make use of the stacking power of the horizontal ghost assuming that other interferences will counteract each other. If the geophone sampling inside the well allows it, one could also apply signal-processing steps to eliminate such interferences. For example the inclined non-physical events could be suppressed using singular value decomposition filtering (Melo et al., 2013), thus lowering the variability inside the UP part.

Using the grid-searching method described above, we estimated a minimum value of ε at $Q_{trial} = 52.5$ during scanning with Q_{trial} from 30 to 100 with a step $d_Q = 0.5$ for the ghost at 0.13 s. Fig. 7 displays the retrieved zero-offset traces before (Fig. 7:a) and after (Fig. 7:b) Q-compensation with the estimated $Q_{trial} = 52.5$. The obtained Q_{trial} is very close to the correct effective $Q_{eff} = 52.3$ of the overburden above the third layer. Fig. 8 presents the simplified flowchart of the proposed method.

In order to further demonstrate the validity of the adapted Q-compensation method we propose to use for vertical wells, we change the velocity and Q in the reservoir layer to $C_p^3 = 1700 m/s$, and $Q_p^3 = 55$ for a monitor survey. In order to monitor the change of Q-value, we apply the adapted Q-compensation method to both vertical-well datasets, i.e., to the base and monitor surveys. Fig. 9 shows the calculated relationship between Q_{trial} and ε for the based survey and the monitor survey. The panels in Fig. 9:a,c indicate the estimated effective Q-value above the third layer, which are effectively the same. The panels in

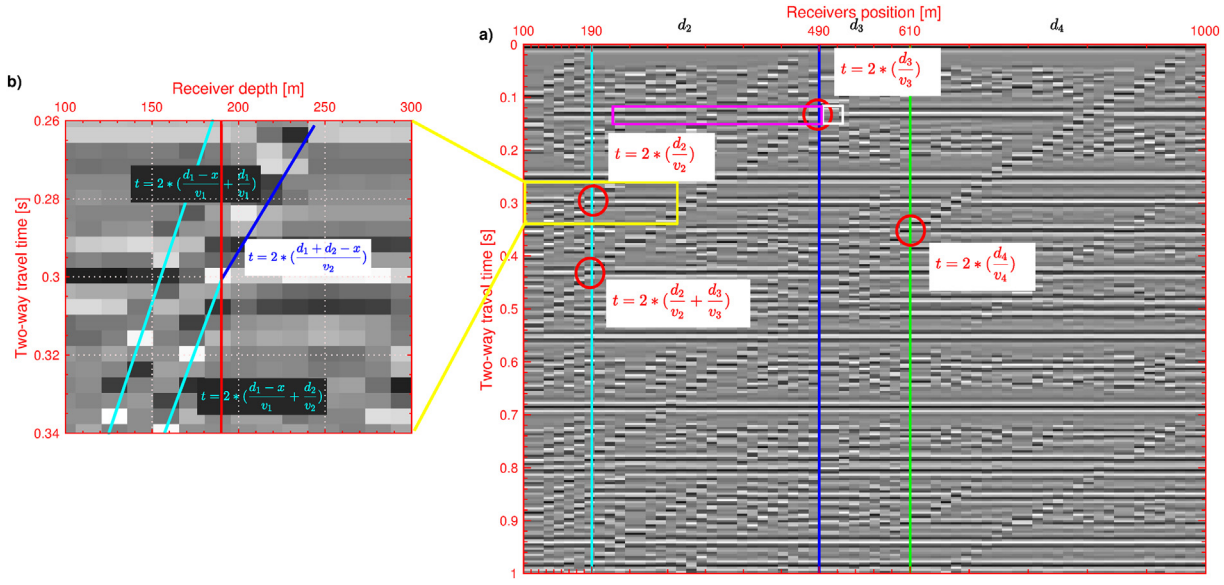

Fig. 6. (a) The retrieved responses using SI applied to the data from the vertical well of the base survey. The kinematic representation for four detected non-physical events are described as $t = 2^* \frac{d_2}{v_2}$ (from the 2*nd* layer), $t = 2^* \frac{d_3}{v_3}$ (from the 3*rd* layer), $t = 2^* \frac{d_4}{v_4}$ (from the 4*th* layer), and $t = 2^* (\frac{d_2}{v_2} + \frac{d_3}{v_3})$ (from the 2*nd* and 3*rd* layer). (b) The zoomed details of the yellow box in (a). The red circles indicate the polarity reversal points on the horizontal ghost arrivals. The kinematic representation for three detected physical events are described as $t = 2^* (\frac{d_1 - x}{v_1} + \frac{d_1}{v_1})$ (the upper lightblue line), $t = 2^* (\frac{d_1 - x}{v_1} + \frac{d_2}{v_2})$ (the lower lightblue line), and $t = 2^* (\frac{d_1 + d_2 - x}{v_2})$ (the blue line). (For interpretation of the references to colour in this figure legend, the reader is referred to the web version of this article.)

Fig. 9:b,d present the effective Q-value above the fourth layer, which indicate a change of the Q-value in the reservoir layer. Thus, we are able to estimate the Q-values from a vertical-well data using the adapted Q-compensation method, that would significantly save the cost in money and computing.

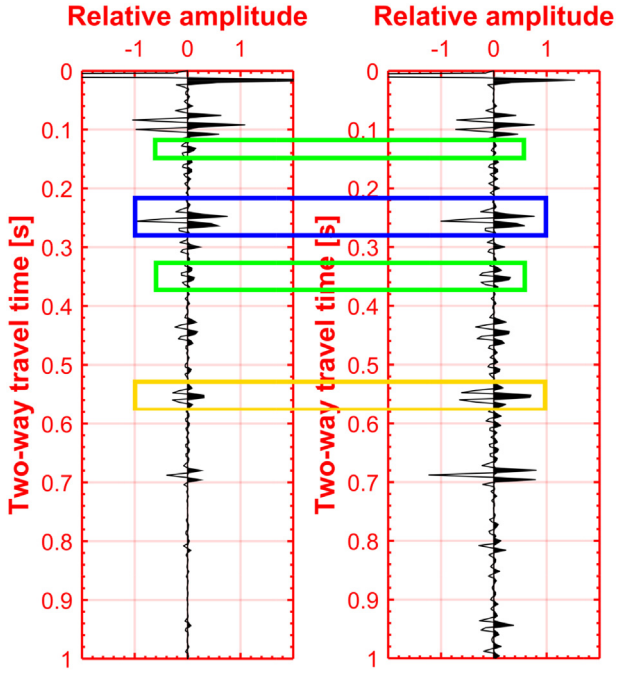

Fig. 7. The retrieved zero-offset reflection trace (a) before and (b) after Q-compensation with the estimated $Q_{trial} = 52.5$. The blue box highlights the physical event, reflection, from the top interface of the second layer; the yellow box highlights the physical event, reflection, from the bottom interface of the second layer. Two green boxes highlight the non-physical events from the third and the fourth layer, respectively. (For interpretation of the references to colour in this figure legend, the reader is referred to the web version of this article.)

We also compare the performance of the SI method we propose against the most commonly used method – the SR method. Here, we follow Matsushima et al. (2016) to calculate Q from the SR representation

$$ln\left[\frac{A(z_2, w)}{A(z_1, w)}\right] = -w\Delta t/2Q + C, \tag{3}$$

where $A(z, w)$ is the amplitude spectrum at angular frequency w and depth z, and Δt is the time difference between the first arrivals from the two receiver depths (z_1, z_2; here, we set $z_1 = 535$ m and $z_2 = 550$ m to calculate the Q in the third layer in the base survey). Using the representation, the linear regression of the left-hand side with respect to frequency yields a slope, k, that is equal to $-\pi\Delta t/Q$. The red and blue dashed lines in Fig. 10a show the spectral amplitude at the depth of z_1 and z_2, respectively. Taking the logarithm of the ratio of the two amplitude spectra gives the left-hand side in eq. 3, which is shown as the thin black line in Fig. 10b. As the method is applied in the frequency domain, it is dependent on the chosen frequency band (Tonn, 1991). Choosing a band shorter or longer than the optimal band would impact adversely the linear regression of the SR. In order to avoid inaccuracies caused by a poor frequency band, we define the most suitable frequency band from 25 Hz to 60 Hz. Using this band, we determine $Q = 54.23$, which is very close to the true value $Q = 55$.

We perform an anti-noise test for both methods to investigate their sensitivity to random noise by adding Gaussian noise to the vertical-well data. The signal-to-noise ratio (SNR) we simulate is $SNR = 50$.

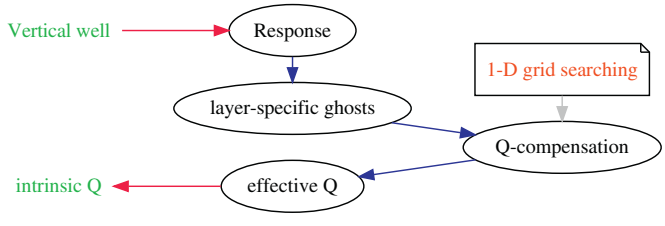

Fig. 8. Flowchart of the Q-estimation procedure for vertical-well data using SI.

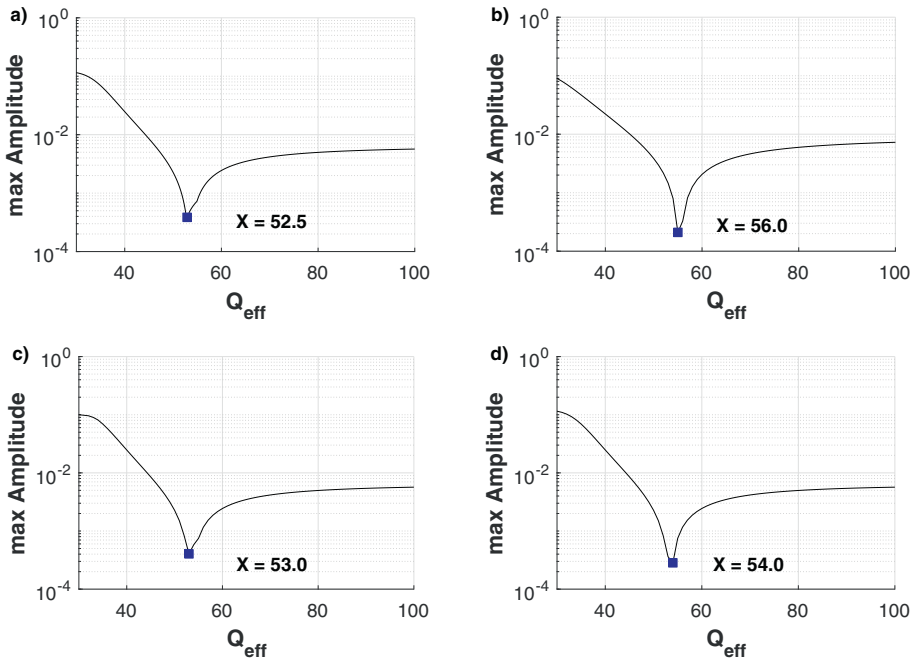

Fig. 9. The obtained relationship between the scanning Q_{trial} and the maximum amplitude ε, (a) for the ghost caused by the third layer in base survey, (b) for the ghost caused by the fourth layer in base survey, (c) for the ghost caused by the third layer in monitor survey, and (d) for the ghost caused by the fourth layer in monitor survey.

This is a high SNR, which should ensure excellent repeatability of stable methods. The solid lines in Fig. 10a show that the random noise introduces slight oscillation in the spectrum, while the thick black line in Fig. 10b indicates the SR amplifies due to the oscillation. The presence of the noise leads to a significantly biased Q-estimation ($Q = 79.49$). We perform 115 random anti-noise tests with the same $SNR = 50$ by applying both the SI and SR methods for Q-estimation. For each of them, we calculate the relative error, i.e., the ratio between the absolute value of the difference between the estimated and the true value and the true value. Fig. 11a shows that the relative errors of the SI method are very stable. They are mostly smaller and less fluctuating than the relative errors of the SR method. This is due to the fact that the cross-correlation operation improves the SNR, that is, not only the cross-correlation between random noises but also the cross-correlation between signal events and random noise is ideally zero, whereas the

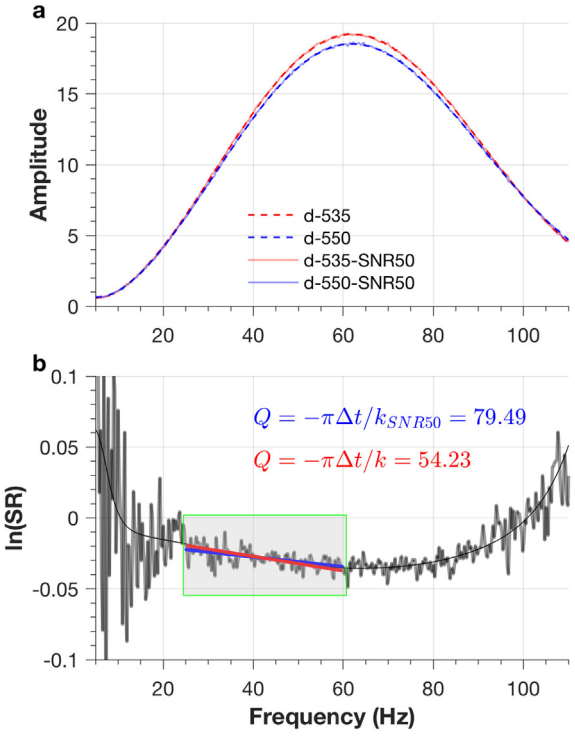

Fig. 10. (a) Spectral amplitude at the depth of $z_1 = 535\ m$ (red lines), $z_2 = 550\ m$ (blue lines) before (dashed lines) and after (solid lines) adding Gaussian noise (SNR = 50). (b) Logarithm of spectral ratio before (thin black line) and after (thick black line) add Gaussian noise. The green box indicates the most suitable frequency band. Two straight lines indicate the linear regression of $\ln\frac{|\bar{A}(z_2,w)|}{|\bar{A}(z_1,w)|}$ before (red) and after (blue) add Gaussian noise. (For interpretation of the references to colour in this figure legend, the reader is referred to the web version of this article.)

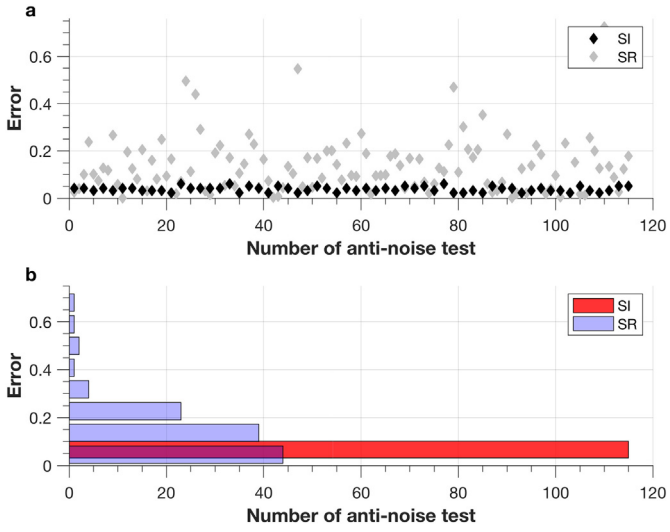

Fig. 11. (a) Relative errors for SR method and SI method in anti-noise test. (b) Relative error histogram distribution for both methods in anti-noise test.

cross-correlation between signal events is enhanced (e.g., Draganov et al., 2010; Matsushima et al., 2016).

The quantity reliability (R) has been used frequently to compare two methods (Tonn, 1991). R is a standard which is weighted for various error limits and is given by

$$R = \frac{E_1/10 + E_2/20 + E5/50}{0.17^{*}N}. \quad (4)$$

where, N is the number of samples ($N = 115$); E_1, is the number of results with error less than 10%; E_2, is the number of results with error less than 20%; and E_5, is the number of results with error less than 50%. From Fig. 11b, we calculate the reliability for the SI and SR method as $R_{SI} = 1.0$ and $R_{SR} = 0.67$, respectively. These corroborate the stability advantage of the method we propose over the SR method.

5. Conclusions

We proposed a method of how to estimate and monitor changes in the layer-specific quality factor (Q) using seismic interferometry by autocorrelation applied to data from a vertical well. The method uses non-physical arrivals (ghosts) appearing in the retrieved result due to the intrinsic losses in the medium. Our method is an adaptation to vertical-well data of a Q-estimation method proposed earlier only for horizontal-well data. We further introduced a quantitative measure – 1-D grid searching – for the estimation of the Q in the Q-compensation procedure to replace the effectively qualitative method originally introduced for the horizontal well. We illustrated how our method works using numerical-modelled data from an active source at the surface and multiple geophones inside a horizontal and a vertical well. When using data from a horizontal well, having also data from a vertical well is imperative for the identification of the retrieved ghosts as such and their connection to a specific subsurface layer. Our adapted Q-estimation procedure eliminated the need for a data from a horizontal well, thus making the Q-estimation a cheaper and practically more feasible procedure. Compared to the performance of the spectral-ratio method, the method we proposed is more stable and reliable in the presence of random noise. We envisage our method to be specifically of interest to wells instrumented with distributed acoustic sensing (optical fibers).

Acknowledgments

The first author thanks Jan Thorbecke for his help in wavefield modelling program. The research of the first author is supported by the National Natural Science Foundation of China (NSFC), under Grant no. 41274142 and the National Nonprofit Institute Research Grant of Institute for Geophysical and Geochemical Exploration, Chinese Academy of Geological Sciences (Grant No. WHS201306). The research of the second author is supported by the Division for Earth and Life Sciences (ALW) with financial aid from the Netherlands Organization for Scientific Research (NWO) with VIDI grant 864.11.009. We thank two anonymous reviewer for their constructive comments that helped improve the manuscript.

References

Aki, K., Richards, P.G., 2002. Quantitative Seismology. 2nd Edn. University Science Books.
Campillo, M., Paul, A., 2003. Long-range correlations in the diffuse seismic coda. Science 299, 547–549.
Chew, W., Liu, Q., 1996. Perfectly matched layers for elastodynamics: A new absorbing boundary condition. J. Comput. Acoust. 4, 341–359.
Draganov, D., Ghose, R., Ruigrok, E., Thorbecke, J., Wapenaar, K., 2010. Seismic interferometry, intrinsic losses and Q-estimation: Geophysical Prospecting. 58 pp. 361–373.
Draganov, D., Ghose, R., Heller, K., Ruigrok, E., 2013. Monitoring changes in velocity and Q using non-physical arrivals in seismic interferometry. Geophys. J. Int. 192, 699–709.
Draganov, D., Ruigrok, E., Ghose, R., Mikesell, D., van Wijk, K., 2015. Quality-factor and reflection-coefficient estimation using surface-wave ghost reflections from subvertical structures. J. Appl. Geophys. 112, 206–214.
Drossaert, F.H., Giannopoulos, A., 2007. A nonsplit complex frequency-shifted pml based on recursive integration for fdtd modeling of elastic waves. Geophysics 72, T9–T17.
Hauge, P.S., 1981. Measurements of attenuation from vertical seismic profiles. Geophysics 46, 1548–1558.
Joshi, S., 2003. Cost/benefits of Horizontal Wells: SPE Western Regional/AAPG Pacific Section Joint Meeting. 9.
Liu, L., Lane, J.W., Quan, Y., 1998. Radar attenuation tomography using the centroid frequency downshift method. J. Appl. Geophys. 40, 105–116.
Matsushima, J., Ali, M.Y., Bouchaala, F., 2016. Seismic attenuation estimation from zero-offset: VSP data using seismic interferometry. Geophys. J. Int. 204, 1288–1307.
McDonal, F., Angona, F., Mills, R., Sengbush, R., Van Nostrand, R., White, J., 1958. Attenuation of shear and compressional waves in Pierre shale. Geophysics 23, 421–439.
Melo, G., Malcolm, A., Mikesell, D., van Wijk, K., 2013. Using svd for improved interferometric greens function retrieval. Geophys. J. Int. 194, 1596–1612.
Parolai, S., 2014. Shear wave quality factor: Qs profiling using seismic noise data from microarrays. J. Seismol. 18, 695–704.
Quan, Y., Harris, J.M., 1997. Seismic attenuation tomography using the frequency shift method. Geophysics 62, 895–905.
Ruigrok, E., 2012. Body-wave seismic interferometry applied to earthquake-and storm-induced wavefield: PhD thesis. TU Delft, Delft University of Technology.
Schuster, G., Yu, J., Sheng, J., Rickett, J., 2004. Interferometric/daylight seismic imaging. Geophys. J. Int. 157, 838–852.
Snieder, R., 2004. Extracting the Green's function from the correlation of coda waves: a derivation based on stationary phase.: physical review E. **69** p. 046610.
Snieder, R., 2007. Extracting the Green's function of attenuating heterogeneous acoustic media from uncorrelated waves. J. Acoust. Soc. Am. 121, 2637–2643.
Stainsby, S., Worthington, M., 1985. Q estimation from ver- tical seismic profile data and anomalous variations in the central north sea. Geophysics 50, 615–626.
Thorbecke, J., Draganov, D., 2011. Finite-difference modeling experiments for seismic interferometry. Geophysics 76, H1.
Tonn, R., 1991. The Determination of the Seismic Quality Factor Q From Vsp Data: a Comparison of Different Computational Methods. Geophys. Prospect. 39, 1–27.
Wang, Y., 2014. Stable Q analysis on vertical seismic profiling data. Geophysics 79, D217–D225.
Wapenaar, K., Fokkema, J., 2006. Green's function representations for seismic interferometry. Geophysics 71, SI33–SI46.
White, R., 1992. The accuracy of estimating q from seismic data. Geophysics 57, 1508–1511.
Zhang, C., Ulrych, T.J., 2002. Estimation of quality factors from cmp records. Geophysics 67, 1542–1547.